Journal of Alloys and Compounds 495 (2010) 360–364

Contents lists available at ScienceDirect

Journal of Alloys and Compounds

journal homepage: www.elsevier.com/locate/jallcom

Nanostructure development during devitrification and deformation

J.H. Perepezko[a,*], S.D. Imhoff[a], R.J. Hebert[b]

[a] University of Wisconsin-Madison, Department of Materials Science and Engineering, 1509 University Ave., Madison, WI 53706,USA
[b] University of Connecticut, Chemical, Materials and Biomolecular Engineering Department, 97 North Eagleville Rd., Storrs, CT 06269, USA

ARTICLE INFO

Article history:
Received 15 July 2008
Received in revised form 27 April 2009
Accepted 8 October 2009
Available online 20 October 2009

Keywords:
Nanostructures
Amorphization
Precipitation
Mechanical alloying

ABSTRACT

The devitrification of amorphous phases can be controlled to yield a nanoscale microstructure based upon either a high density of nanocrystals dispersed in an amorphous matrix or a completely nanocrystalline solid. For both rapidly solidified marginal glass forming alloys and slowly cooled bulk glass forming alloys, the high nanocrystal densities are related to nucleation reactions that are sensitive to the initial as-prepared state of the amorphous phase. For example, nucleation densities of 10^{21} m^{-3} can be enhanced to 10^{23} m^{-3} by selective doping of Al-based glasses and the glass forming ability of bulk amorphous alloys is known to be sensitive to minor impurities. The addition of only 1 at.% of Cu to amorphous Al–Sm–Ni or Al–Y–Fe alloys is an effective microstructure control by narrowing the size distribution of Al nanocrystals and reducing the average size of the nanocrystals from 10 nm to about 7.5 nm while increasing the particle number density. Calorimetry and microstructural analyses of the primary Al crystallization reaction suggest that the addition of Cu modifies the atomic arrangement and induces structural heterogeneities based upon medium range order (MRO) that can act as nucleation sites. The strong composition dependence of the crystallization reactions and resulting microstructures reflect not only underlying thermodynamic constraints, but also indicates a strong composition dependence of the amorphous phase atomic arrangement. These features point to a central role for heterogeneities in the evolution of nanoscale microstructures. During nanostructure synthesis by deformation of multilayers the thermodynamic constraints are also important, but the co-deformation of layers governs the generation of interfacial area that allows for the nanoscale alloying reaction. Moreover, kinetics studies have also revealed that the governing reactions often proceed under transient conditions and can lead to relatively stable and robust nanoscale microstructures.

1. Introduction

The major attention that is currently focused on nanostructured materials has generated numerous synthesis methods, but the vast majority of these innovations yield microscopic material quantities. While there are many electronic and photonic applications where small material quantities or modified surfaces are satisfactory, structural applications require large scale and reproducible synthesis methods. For this purpose devitrification reactions [1] and intense deformation [2] are established as most effective techniques. At the same time the achievement of reproducible nanostructured microstructures implies a control over the reactions which in turn requires an understanding of the atomistic mechanisms.

For devitrification reactions the remarkably high nucleation number densities for primary crystallization have been related to different nanoscale heterogeneities. For example, with Fe base amorphous alloys such as FINEMET, an Fe–Si–B–Nb–Cu alloy, Cu aggregates develop into a precursor site for primary crystallization of α-Fe [3–6]. With amorphous Al alloys primary crystallization also yields a high number density of nanocrystalline Al, but there does not seem to be any solute aggregation as the origin [7]. However, a nanoscale heterogeneity has been observed in the form of medium range order (MRO) [8]. It is also apparent that the composition dependence of the crystallization onset temperature, T_x, is much steeper for amorphous Al alloys than is typical for metallic glass alloys [1]. In fact, another form of composition sensitivity is also apparent in the strong shift in T_x with minor solute doping. For example, in Al–Ni–Sm the substitution of Ni by 1%Cu causes T_x to decrease by almost 60 K [9]. In addition, Latuch et al. [10] and Inoue [11] have looked at the Al–Y–Ni base system with Cu and Co additions where similar changes in the crystallization temperature occur. The composition sensitivity of the primary nanocrystallization reaction is of fundamental importance, but also has a practical impact on the achievement of reproducible nanoscale microstructures.

During intense deformation of crystalline multilayers or amorphous ribbons nanoscale microstructures are possible by different

* Corresponding author. Tel.: +1 608 263 1678.
E-mail address: perepezk@engr.wisc.edu (J.H. Perepezko).

0925-8388/$ – see front matter © 2009 Elsevier B.V. All rights reserved.
doi:10.1016/j.jallcom.2009.10.051

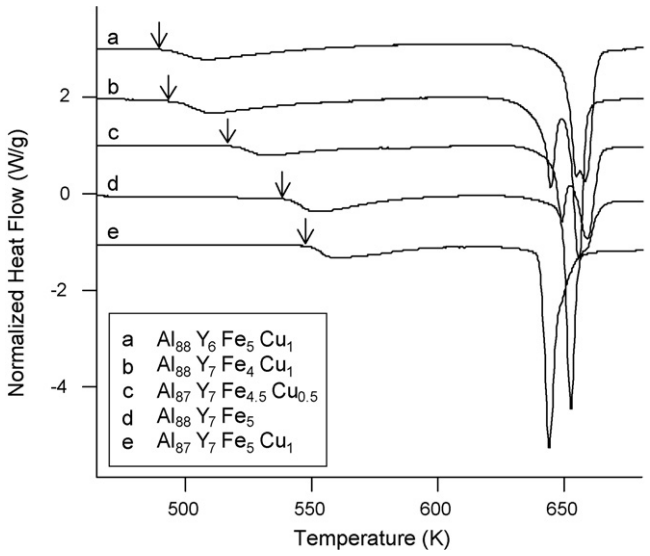

Fig. 1. DSC thermogram showing the difference in crystallization onset for Al–Y–Fe with and without copper substitution for different components.

driven reaction pathways. For example, the nanoscale alloying that develops at multilayer interfaces can yield nanocrystalline alloys or metallic glass. In this case both the process and system response are important in alloying and phase development [12,13]. On the other hand for deformed amorphous ribbon different reactions ranging from nanocrystallization to a change in phase selection are possible [14,15]. Since deformation of amorphous phases involves the generation and propagation of shear bands the range of response suggests that the interaction between shear bands and an initial atomic configuration in the amorphous phase is important.

In the current work several highlights are discussed relating to nanostructure development during deformation and devitrification. A perspective on nanocrystal nucleation during devitrification is considered in terms of the role of MRO. In addition some new observations on deformation induced alloying and devitrification are examined to provide some insight into the governing mechanisms.

2. Primary crystallization

Microstructures based upon a dispersion of primary nanocrystals in an amorphous matrix greatly affect the mechanical and corrosion properties. Whether mechanically driven or quenched into a glass, forging a connection between the state of a precursor glass and the resulting microstructure after primary crystallization is an important but challenging goal. Dopant level additions of Cu for Fe in $Al_{88}Y_7Fe_5$ are shown, in Fig. 1, to enhance nucleation with respect to temperature, shifting the primary crystallization temperature from 549 to 490 K during continuous heating at 20 K/min and exemplifying the sensitivity of crystallization onset temperature and nanocrystal number density to composition. Furthermore, it has been found that the same doping level not only changes the crystallization temperature, but also changes the number density and size of nucleated crystals as illustrated in Fig. 2. This phenomena is observed not only in the Al–Y–Fe system, but has also been studied in Al–Ni–Sm [9], Al–Y–Ni [16], and Al–Y–Ni–Co–(Cu,Pd) [11,17]. In the case of the aluminum alloys mentioned, atom probe studies have found no evidence for copper clustering, as in iron glasses, and have in fact shown that the primary crystals contain no copper [9]. Similar effects have been reported for Ag, Au and other transition metal additions [18]. This type of behavior could be explained by an increase in the heterogeneous site density and in fact TEM evidence and nucleation kinetics analysis point toward increased site density in the form of medium range order regions.

Fluctuation electron microscopy, FEM, allows for observation of new details concerning the heterogeneous nature of atomic arrangements in a glass [19]. By analyzing the variance in TEM image contrast within an amorphous sample, regions have been identified that exhibit aluminum-like order on sub nanometer size scales [20]. Previous study on $Al_{92}Sm_8$ amorphous samples has determined that the ordering is like that of FCC aluminum and not rare earth centered icosahedra or the intermetallic $Al_{11}Sm_3$ phase [8]. If local ordering is incompatible with the nucleating phases

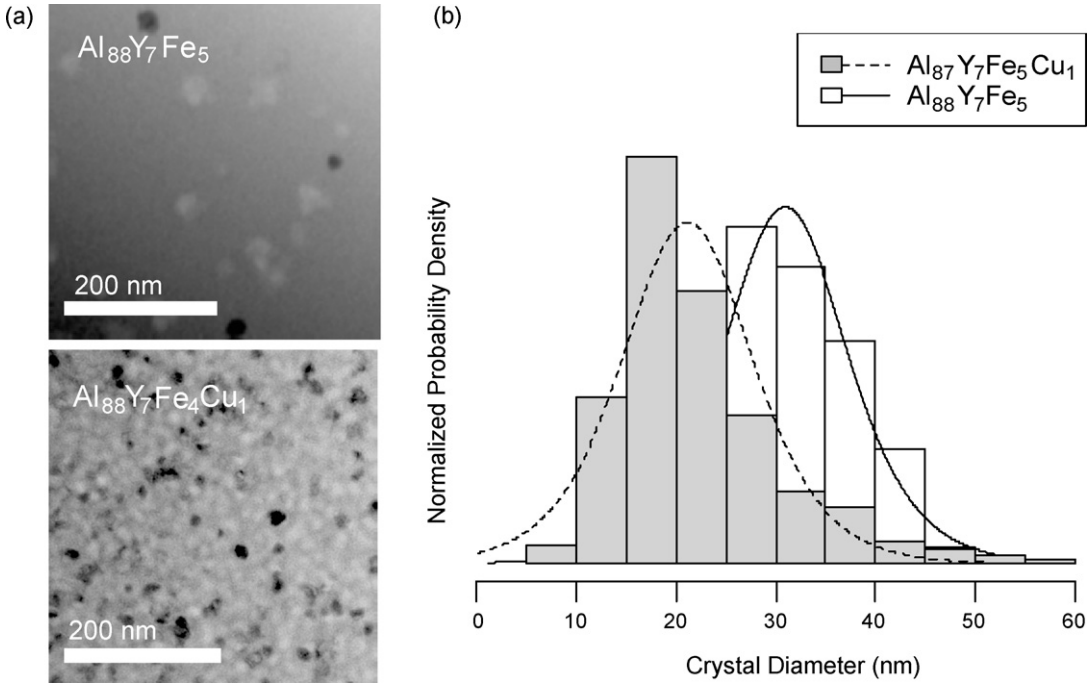

Fig. 2. (a) Bright-field micrographs and (b) nanocrystal population size statistics for $Al_{88}Y_7Fe_5$ and $Al_{88}Y_7Fe_5Cu$.

then the activation barrier could effectively be increased, which may explain why the thermodynamically preferred intermetallic phase is not the first to crystallize upon heating [21]. Most recent findings have shown that these regions of order change in number density, overall volume fraction, and possibly size, with doping [17]. In as spun ribbons of $Al_{88}Y_7Fe_4Cu_1$, there is nearly a two fold increase in the overall volume fraction of amorphous matrix which has significant medium range ordering and the number density of the MRO regions approaches 10^{27} m^{-3}.

In order to examine the kinetic changes induced by doping, calorimetric and stereological analyses were conducted. The DSC continuous heating results for $Al_{88}Y_7Fe_5$ and $Al_{88}Y_7Fe_4Cu_1$ samples in Fig. 1 show typical primary crystallization behavior with an initial exotherm representing the development of Al nanocrystals and a final exotherm for crystallization of an Al and intermetallic phase mixture. It is interesting to note that the secondary reaction also changes both in temperature and character of the signal. While this shift is not as dramatic as the primary crystallization, it serves to indicate that small changes in composition affect the character of reaction and the onset reaction temperature sensitivity. It is evident that the addition of Cu depresses the onset of primary crystallization by approximately 60 °C. A further comparison of the crystallization behavior was obtained by annealing at temperatures about 30 °C below the onset of crystallization. Microstructural analysis, as shown in Fig. 2, reveals that Cu substitution increases the number of nanocrystals fourfold and decreases their average size by 50% resulting in $Al_{88}Y_7Fe_4Cu_1$ having roughly 1.5 times more crystallized material than $Al_{88}Y_7Fe_5$.

Similar to the Al–Y–Fe, selective substitutions of Cu for Ni in $Al_{88}Ni_{8-x}Sm_4Cu_x$ melt-spun ribbon samples (x = at.% Cu, ranging from 0.2 → 1 at.%) shift the calorimetrically measured onset of primary crystallization to successively lower temperatures with increasing amount of Cu substitution (Fig. 3). The enthalpy of primary crystallization does not change appreciably with Cu substitution level indicating that the volume of amorphous precursor material transforming to primary Al nanocrystals remains essentially constant. Furthermore, the shape of the primary exothermic signal deviates from a sharp peak to a more gradual depression extending over a wider temperature range. Microstructure analysis of ribbon samples of $Al_{88}Ni_8Sm_4$ and $Al_{88}Ni_7Sm_4Cu_1$ annealed for 30 min at the onset of primary crystallization for each composition, 154 and 104 °C respectively, indicates that the average size of the primary phase nanocrystals is reduced by nearly 25% from about 10 nm to about 7.5 nm with Cu substitution. The estimated nanocrystal number density increased from 9×10^{21} to 1.6×10^{22} m^{-3} with substitution of 1 at.% Cu for Ni in the base alloy composition.

Since the doping effect on primary crystallization is observed in multiple systems and in at least two of these systems the identification of MRO changes has been confirmed, it is important to consider the possible role of MRO in the primary reaction. An analysis to determine whether the origin of the MRO regions is related to the quenching in of the cluster concentration can be considered in terms of $C(n) = C_0 \exp(-\Delta G_n/k_B T)$, where $C(n)$ is the population of clusters of size n, C_0 is the monomer concentration and ΔG_n is the energy barrier for a cluster of n atoms. A parallel tangent construction was utilized to obtain ΔG_V [22] and subsequently the activation barrier, ΔG_n through the relationship of $\Delta G_n = [4\pi(3n\upsilon_a/(4\pi))^{2/3}\sigma + n\Delta G_V]$, where υ_a is the atomic volume (1.65×10^{29} m^{-3}) and σ is the interfacial energy as calculated with the Spaepen model [23] as 0.104 J/m^3. Fig. 4 shows that the "quenched-in" temperature to achieve the measured number density of MRO regions is significantly below room temperature and inappropriate for accounting for the observed NC density. Estimates of $C(n)$ from a the linked flux [24] analysis result in even less favorable values. This suggests that the MRO regions may be representative of the inherent amorphous phase atomic configuration rather than a fluctuation clustering process.

The usual fluctuational clustering processes have proven deficient to explain the number density so that it is reasonable to look for an additional feature aiding in nucleation. If it is assumed that the MRO regions are the key feature in considering the high nanocrystal densities, then a more complete kinetic picture can be drawn. For this analysis an initial model based upon homogeneous nucleation was inconsistent with the observed nucleation densities. Instead, the implementation of a seeded nucleation model in which the Al-like MRO regions are assumed to aid in the nucleation process was found to be consistent with the observations. Briefly, the kinetics model is based upon the calculation of ΔG_V and σ as described earlier but with the MRO considered as an internal catalyst that is enveloped by the evolving Al nanocrystal. Under this heterogeneous process the volume and the nucleation barrier, ΔG^*, for Al nanocrystal nucleation is reduced considerably for an MRO size of 0.370 nm. For example, at 550 K, $\Delta G^*/kT$ is reduced to 26 for catalyzed nucleation. Within this model, the steady state nucleation

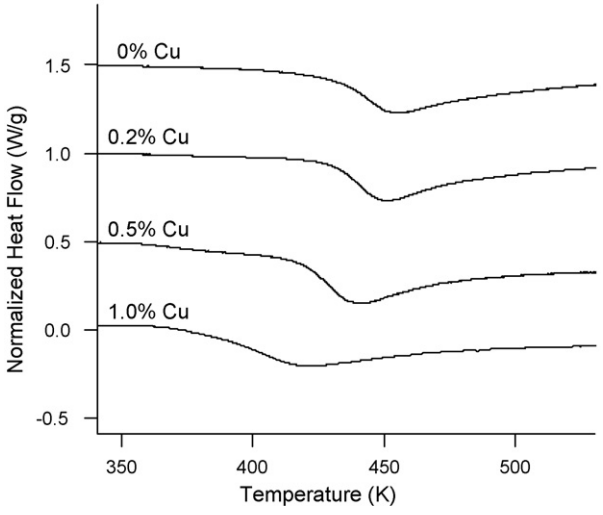

Fig. 3. DSC traces (dT/dt = 20 K/min) of $Al_{88}Ni_{8-x}Sm_4Cu_x$ MSR samples; as the crystallization onset shifts to lower temperatures with greater Cu addition, integrated crystallization enthalpy remains constant.

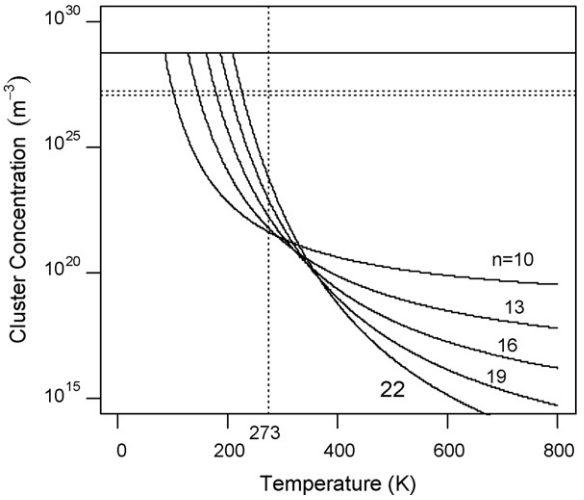

Fig. 4. Calculated equilibrium cluster concentrations for a variety of clusters of n atoms. MRO regions are indicated by horizontal dashed lines. The vertical dashed line indicates 0 °C.

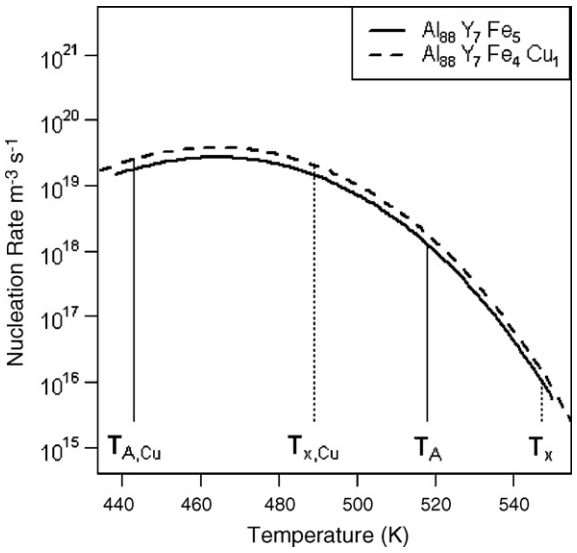

Fig. 5. The calculated steady state nucleation rate with temperature for Cu doped and undoped $Al_{88}Y_7Fe_5$ samples. T_A is the annealing temperature and T_x is the crystallization temperature during constant heating (20 K/min).

rate [25] may be evaluated from

$$J_{SS} = \rho\beta Z \exp\left(-\frac{\Delta G^*}{kT}\right) \quad (1)$$

where ρ is the MRO site density and Z is the Zeldovich factor which typically varies between 0.1 and 1. The attachment frequency, β, is determined by $\beta = 4\pi r^{*2} D X_0 a^{-4}$ where r^* is the critical nucleus size, D is the diffusivity [22,26], X_0 is the aluminum concentration of the matrix, and a is the jump distance.

The temperature dependence of J_{ss} is presented in Fig. 5. Interestingly, the steady state nucleation rates showed a peak at temperatures below the constant heating crystallization onset temperatures for both $Al_{88}Y_7Fe_5$ and $Al_{88}Y_7Fe_4Cu$. The clear deviation between the crystallization start temperature under heating conditions and the temperatures which yield a maximum in nucleation rate suggests that transient effects are important during the nucleation process. In order to explore these differences, a thorough study of the nucleation rate at 225 °C and 245 °C was conducted with $Al_{88}Y_7Fe_5$ in which samples were annealed at intervals between 1 and 10 min and the microstructures were investigated. It was found that the first discernable crystals were observed at 10 min at 225 °C and approximately one minute at 245 °C, corresponding to a number density of roughly 10^{20} m^{-3}. These data directly confirm an incubation time during which the system moves toward steady state. The transient effect on nucleation can be incorporated by evaluating the time dependent nucleation rate $J(t) = J_{ss}\exp(-\tau/t)$ where $\tau = (\beta Z)^{-1}$. With this refinement it is possible to account for the change in crystallization onset temperature with doping if there is a change in the corresponding incubation time. However, it is also expected that potential modifications in the medium range order and changes in the bonding character on a local level [21,27], that will also impact the transport and nucleation behavior.

3. Deformation induced mixing

The response of materials to intense deformation is expressed through different reaction pathways depending on the initial state. For crystals undergoing plastic deformation it is well established that in single phase materials there is a structure refinement to nanoscale grain sizes and high dislocation densities [2]. For mixtures of different materials various alloying reactions can develop leading to stable or metastable solid solutions, intermediate phases or metallic glass products. With an initial amorphous phase, intense deformation yields shear banding that in some cases can interact with the local atomic configurations to result in nanocrystallization [14,28,29]. While the final structures are well established, the reaction paths and mechanisms are in most cases uncertain.

Some insight on the possible reaction paths has been developed from simulation studies on driven systems. With crystalline multilayers the interplay of process and control parameters results in different microstructural patterns ranging from full mixing even for immiscible components to self organized motifs [30–35]. For the conditions of the simulations that involve small groups of atoms and very high strain rates the mixing has been called superdiffusive since the time dependence is linear rather than the thermally driven parabolic kinetics [30]. There are also computational studies of dislocation behavior in deformed multilayers that indicate several types of interaction [36–38]. Dislocations within the interface contribute to multilayer sliding while dislocations within the layers can intersect the interface to create steps or translate into an adjacent layer. These characteristics can provide opportunities for atomic scale interfacial mixing during deformation as the multilayer structure is refined.

For the deformation induced reaction in multilayers it is evident that components that form an isomorphous system offer a number of advantages. For example, in a Ni/Cu multilayer there is background thermodynamic and diffusion data [37,39,40] available for the interpretation of the intermixing. During the repeated cold rolling and folding process an initial laminar structure is iteratively refined by the action of the rollers to yield a high interfacial area that increases according to a sigmoidal function. When the sample is in a nanometer scale multilayer structure, the amount of internal interface area for phase reaction is large [40].

Initial work has shown that intense deformation yields a significant layer reduction. For Cu–Ni multilayers after 50 rolling passes, the multilayer has a mean spacing of about 88 nm, for a relative specific interfacial area (i.e. interfacial area/initial interfacial area) of about 280. Moreover, X-ray diffraction measurements of the lattice parameters that are presented in Fig. 6 also indicate that alloying does occur with increasing strain and seems to occur in stages. For the $Cu_{60}Ni_{40}$ multilayer there is an initial alloying up to a composition of $Cu_{70}Ni_{30}$ that reflects the asymmetric mixing. This composition remains for a period of increasing strain before the disappearance of the Ni layers and the completion of mixing to the nominal composition of the initial multilayer. The solid solution becomes the only phase present at around 50 passes.

The behavior for the $Cu_{40}Ni_{60}$ multilayer is a bit different than that in the $Cu_{60}Ni_{40}$ sample even though the layer refinement is similar, Fig. 6. There appears to be a trend for the Cu layer to exhibit dissolution of Ni as an initial stage that continues with increasing deformation until the alloyed layer develops at about 35 passes. Again, with the disappearance of the Ni layers, the solid solution is the only phase present at about 50 passes.

The width of the copper and nickel peaks rise in a very similar fashion as grain size decreases. The solid solution peak however starts out very broad comprising essentially the entire breadth of composition between the two pure elements. With continued deformation, the peak width decreases. During this time the layers are undergoing mixing. Since the main source of peak sharpening in the solid solution is the reduction of composition gradient, this provides further evidence of mixing stages. At the same time there is a marked increase in the relative volume of solid solution present. Once all the copper has been consumed continued deformation can drive the system to dissolve the remaining nickel and reach the nominal composition of the multilayer.

A further kinetics analysis is necessary for the complete modeling of the reactions, but some initial observations can be made

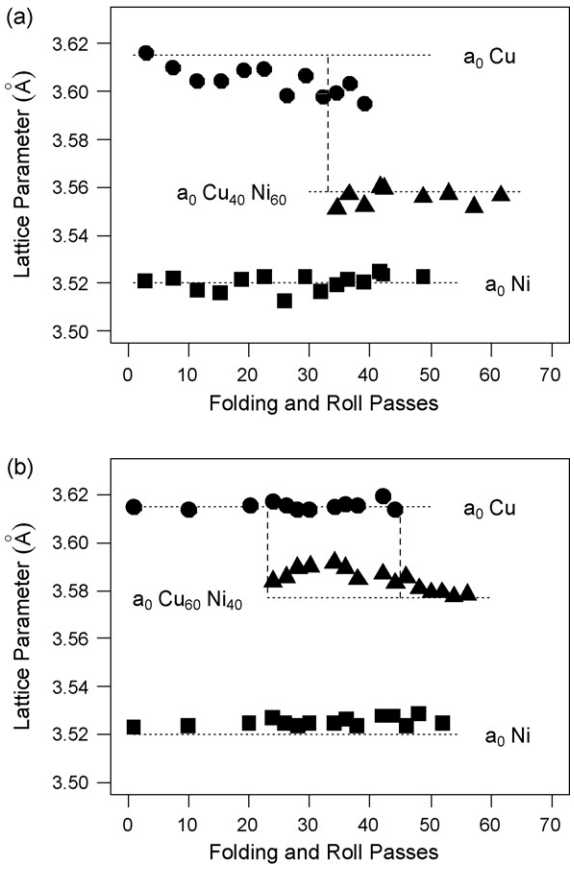

Fig. 6. Lattice parameter measurements for a Cu–Ni multilayer as a function of strain rate (a) $Cu_{60}Ni_{40}$ (b) $Cu_{40}Ni_{60}$.

that relate to the driven system behavior. For example, from the reported diffusivities D_{Ni}/D_{Cu} is about 10^{-5} at room temperature which would indicate a much stronger asymmetry that observed and reported in simulations [39]. Moreover, the homogenization of the alloy from 30 to 50 passes over an active deformation time of 60 s for a strain rate of $0.4\,s^{-1}$ cannot be accomplished by thermal diffusion, but is possible for an effective temperature of about 345 °C that suggests an important role for deformation enhanced transport.

4. Summary

Amorphous Al alloys present a number of intriguing challenges to the contemporary understanding of amorphous phase formation and stability. While the widely accepted guidelines for amorphous phase formation seem to apply to component selection, the typical Al-rich compositions and relatively high crystallization temperatures suggest another role for the specific solutes in facilitating stability. At the same time, the strong composition dependence of the thermal stability and the remarkably high nucleation density developed during primary crystallization are unusual. Moreover, structural determinations reveal a heterogeneous structure that is characterized by a high level of Al-like MRO. When these characteristic features are considered together it is evident that the conventional kinetics analysis should be modified to take account of the heterogeneous behavior. A model to incorporate the inherent structure of local MRO regions as sites for the initiation of Al nanocrystals has been formulated that accounts for the observed nucleation density and the crystallization behavior during annealing. From the analysis it is also evident that transient kinetics plays an important role in the evolution of the nanoscale microstructure during primary crystallization. Similarly, nanoscale processes control the deformation induced reaction of elemental multilayers. The initial stage of the reaction develops mainly by an extensive refinement of the multilayer spacing. Accompanying the layer refinement, there is a steep increase in the relative interfacial area per unit volume that yields a detectable mixing volume. During the later stage of reaction the convergence of the layer refinement with the mixing volume yields full alloying that is facilitated by deformation enhanced transport.

Acknowledgement

R.J.H. gratefully acknowledges the support from the NSF (CMMI-0700377). J. Lyons is thanked for his help with experimental work.

References

[1] A. Inoue, Progress Prog. Mater. Sci. 43 (1998) 365.
[2] C. Suryanarayana, Prog. Mater. Sci. 46 (2001) 1.
[3] K. Hono, D.H. Ping, M. Ohnuma, H. Onodera, Acta Mater. 47 (1999) 997.
[4] K. Suzuki, A. Makino, A. Inoue, T. Masumoto, J. Appl. Phys. 70 (1991) 6232.
[5] Y. Yoshizawa, S. Oguma, K. Yamauchi, J. Appl. Phys. 64 (1988) 6044.
[6] K. Suzuki, N. Kataoka, A. Inoue, A. Makino, T. Masumoto, Mater. Trans., JIM 31 (1990) 743.
[7] K. Hono, Y. Zhang, A. Inoue, T. Sakurai, Mater. Trans., JIM 36 (1995) 909.
[8] W.G. Stratton, J. Hamann, J.H. Perepezko, P.M. Voyles, X. Mao, S.V. Khare, Appl. Phys. Lett. 86 (2005) 141910.
[9] Y. Zhang, P.J. Warren, A. Cerezo, Mater. Sci. Eng., A 327 (2002) 109.
[10] J. Latuch, A. Kokoszkiewicz, H. Matyja, Mater. Sci. Forum 269–272 (1998) 755.
[11] D.V. Louzguine, A. Inoue, J. Mater. Res. 17 (2002) 1014.
[12] R.J. Hebert, J.H. Perepezko, Scr. Mater. 50 (2004) 807.
[13] R.J. Hebert, J.H. Perepezko, Scr. Mater. 49 (2003) 933.
[14] R.J. Hebert, J.H. Perepezko, Metall. Mater. Trans. A 39A (2008) 1804.
[15] J.H. Perepekzo, R.J. Hebert, G. Wilde, Mater. Sci. Eng., A 375–377 (2004) 171.
[16] S.J. Hong, P.J. Warren, B.S. Chun, Mater. Sci. Eng., A 304–306 (2001) 362.
[17] D.V. Louzguine-Luzgin, A. Inoue, J. Mater. Res. 21 (2006) 1347.
[18] K.S. Bondi, A.K. Gangopadhyay, Z. Marine, T.H. Kim, A. Mukhopadhyay, A.I. Goldman, W.E. Bhuro, K.F. Kelton, J. Non-Cryst. Solids 353 (2007) 4723.
[19] P.M. Voyles, J.M. Gibson, M.M.J. Treacy, J. Electron Microsc. 49 (2000) 259.
[20] W.G. Stratton, S.I. Imhoff, J.H. Perepezko, P.M. Voyles, to be published.
[21] A. Sadoc, O. Heckmann, V. Nassif, O. Proux, J.-L. Hazemann, L.Q. Xing, K.F. Kelton, J. Non-Cryst. Solids 353 (2007) 2758.
[22] D.R. Allen, J.C. Foley, J.H. Perepezko, Acta Mater. 46 (1998) 431.
[23] F. Spaepen, Solid State Phys. 47 (1994).
[24] K.C. Russell, Acta Metall. 16 (1968) 761.
[25] H.I. Aaronson, J.K. Lee, in: H.I. Aaronson (Ed.), Lectures on the Theory of Phase Transformations, TMS, Warrendale, PA, 2001, pp. 165–229.
[26] R. Hebert, Deformation-induced synthesis of amorphous alloys, University of Wisconsin-Madison, 2003.
[27] K. Saksi, P. Jovari, H. Franz, J.Z. Jiang, J. Appl. Phys. 97 (2005) 113507.
[28] C.A. Schuh, T.C. Hufnagel, U. Ramamurty, Acta Mater. 55 (2007) 4067.
[29] R.J. Hebert, J.H. Perepezko, H. Rosner, G. Wilde, Scr. Mater. 54 (2006) 25.
[30] P. Bellon, R.S. Averback, S. Odunuga, Y. Li, Krasnochtchekov, Phys. Rev. Lett. 99 (2007) 110602.
[31] F. Delogu, Acta Mater. 56 (2008) 2344.
[32] S. Odunuga, Y. Li, P. Krasnochtchekov, P. Bellon, R.S. Averback, Phys. Rev. Lett. 95 (2005) 045901.
[33] J.D. Hahn, F. Wu, P. Bellon, Metall. Mater. Trans. A 35 (2004) 1105.
[34] P. Bellon, R.S. Averback, Phys. Rev. Lett. 74 (1995) 1819.
[35] Y. Sun, G.R. Purdy, Can. Metall. Q. 45 (2006) 131.
[36] A. Misra, J.P. Hirth, R.G. Hoagland, Acta Mater. 53 (2005) 4817.
[37] J. Wang, R.G. Hoagland, J.P. Hirth, A. Misra, Acta Mater. 56 (2008) 3109.
[38] M.A. Shehadeh, G. Lu, S. Banerjee, N. Kioussis, N. Ghoniem, Philos. Mag. 87 (2007) 1513.
[39] J.-M. Roussel, P. Bellon, Phys. Rev. B 73 (2006) 085403.
[40] D. Mitlin, A. Misra, T.E. Mitchell, J.P. Hirth, R.G. Hoagland, Philos. Mag. 85 (2005) 3379.